Single neurons act as a memory buffer for space

Babak Saber Marouf [1 2 3], Antonio Reboreda [2 3], Frederik Theissen [2 3], Rahul Kaushik [4], Magdalena Sauvage [3 5 6], Alexander Dityatev [4 5 6], Motoharu Yoshida [2 3 6]

Affiliations

[1]Institute of Physiology, Medical Faculty, Otto-Von-Guericke University, 39120 Magdeburg, Germany.

[2]Cognitive Neurophysiology, German Center for Neurodegenerative Diseases (DZNE), 39120 Magdeburg, Germany.

[3]FAM Department, Leibniz Institute for Neurobiology (LIN), 39118 Magdeburg, Germany.

[4]Molecular Neuroplasticity Group, German Center for Neurodegenerative Diseases (DZNE), 39120 Magdeburg, Germany.

[5]Medical Faculty, Otto-von-Guericke University (OvGU), 39120 Magdeburg, Germany.

[6]Center for Behavioral Brain Sciences (CBBS), 39106 Magdeburg, Germany.

Summary

The brain's ability to briefly retain information is believed to depend on persistent neural firing. Historically, persistent firing has been attributed to recurrent synaptic networks, in which neural activity reverberates. This view aligns with the widely accepted principle that neurons generate action potentials only in response to sufficiently strong input, and therefore do not serve as memory components. Here, we present evidence challenging this view, demonstrating in behaving mice that individual hippocampal neurons can sustain persistent firing, acting as a memory buffer for spatial representation. We first demonstrate that TRPC4 ion channel silencing selectively disrupts the capability of individual neurons to persistently fire using *in vitro* recordings in mice. This manipulation impairs spatial working memory performance, and significantly and selectively reduces persistent firing *in vivo* during the maintenance (delay) period of the task. Despite general belief that persistent firing maintains working memory contents, we find persistent firing to reflect continuous firing of spatial cells coding for spatial information, suggesting that maintenance of spatial representation in the hippocampus may depend on intrinsic cellular mechanism. We further demonstrate that TRPC4 silencing selectively affect hippocampal spatial coding where mice stayed in a place for an extended time (start and goal areas), pointing out the specific role of intrinsic cellular mechanisms of persistent firing in the retention of spatial information and potential coexistence of intrinsic cellular mechanism with attractor dynamics. Finally, task performance correlated with the strength of persistent firing in the goal area, suggesting that maintained goal representation in the hippocampus is crucial for the task performance. These findings redefine neurons as active contributors to information retention beyond their conventional role as passive input-output units, potentially reshaping our general understanding of brain computation.

Introduction

Persistent neural activity is widely recognized as a cellular mechanism underlying short-term information storage critical for working memory, path integration, and other cognitive processes[1–4]. Building on the foundational concepts of Lorente de Nó and Hebb, persistent activity has been attributed to reverberatory dynamics within recurrent synaptic networks[5,6]. This view aligns with the prevailing model of neurons as passive elements generating action potentials only when synaptic inputs exceed a threshold. However, evidence suggests that individual neurons may independently sustain firing, challenging this network-centric model.

Studies have shown that neurons can continue firing after a brief trigger independent of synaptic input, a phenomenon referred to as intrinsic persistent firing[7–10]. Intrinsic persistent firing often depends on ion channels activated by neuromodulators, such as acetylcholine, which are vital for memory and other cognitive functions[11–14]. Theoretical studies have demonstrated potential roles of the intrinsic mechanisms underlying persistent firing in working memory and path integration[15,16], suggesting that "hybrid models" including intrinsic persistent firing in addition to network mechanism outperform pure network models by increasing stability and robustness[17–19]. However, whether intrinsic persistent firing influences *in vivo* neural activity, sustains information, and supports cognitive function remains unclear because the effects of disrupting this property have not been examined in living animals[20,21].

Here, we developed a mouse model in which intrinsic persistent firing was disrupted, and recorded *in vivo* during a spatial working memory task for the first time. Our findings challenge the conventional view of neurons as passive input-output elements, demonstrating that individual neurons actively sustain information *in vivo*. This conceptual advance has significant implications for computational models of brain function and disorders, such as Alzheimer's disease and aging, where compromised cholinergic neuromodulation is associated with deficits in spatial navigation and working memory.

72 # Results

73 **TRPC4 KD suppresses intrinsic persistent firing in vitro**

74 We developed an shRNA TRPC4 channel knockdown (TRPC4 KD) virus and a control virus with a
75 scrambled sequence (Scrambled) to test the role of intrinsic persistent firing *in vivo* (see Methods; Fig.
76 1A)[22]. The mice received bilateral injections of either virus into the CA1 region (Fig. 1B). First, a loss
77 of intrinsic persistent firing was confirmed using *in vitro* patch-clamp recordings of hippocampal CA1
78 cells in the presence of the cholinergic receptor agonist carbachol[13,23] (10 μM; Fig. 1C). Percentages of
79 cells responded with persistent firing, the frequency of persistent firing and membrane depolarization
80 were significantly lower in the TRPC4 KD group than in the two control groups (Fig. 1D-F). Basic
81 properties of TRPC4 KD cells, such as the resting membrane potential, input resistance, adaptation
82 index, and intrinsic excitability, did not significantly differ from those in the control groups (except for
83 intrinsic excitability measured with 100 pA current injection, Kruskal–Wallis test, $p = 0.0193$, Chi-sq
84 $= 7.89$, df = 2; Table 1). In summary, TRPC4 KD significantly decreased the ability of individual cells
85 to support persistent firing while preserving basic cellular properties.

86

87 **TRPC4 KD impairs spatial working memory**

88 Second, the effect of TRPC4 KD on spatial working memory was assessed by a delayed non-match-to-
89 sample paradigm using an automated T-maze (Fig. 1G-I; Supplementary Fig. 1). The scrambled control
90 group mice consistently performed approximately 80% correctly from day two. On the other hand, the
91 performance of the TRPC4 KD group remained approximately 60% correct over the ten days of testing
92 (Fig. 1J). Group comparisons demonstrated that hippocampal TRPC4 KD significantly impaired
93 working memory performance compared to scrambled control mice (Fig. 1K). These results indicate
94 that TRPC4 channels in CA1 neurons are necessary for spatial working memory.

95

96 **TRPC4 KD suppresses *in vivo* persistent firing**

97 Classical theory and evidence suggest that persistent firing supports memory maintenance[24–26]. We
98 tested whether TRPC4 KD affected persistent firing in the T-maze using *in vivo* recordings. We

observed cells with increasing firing rates during the delay (maintenance) period (0–30 s; orange line, Fig. 2A). To quantify such increased firing, we calculated the z-scored firing rate of individual cells

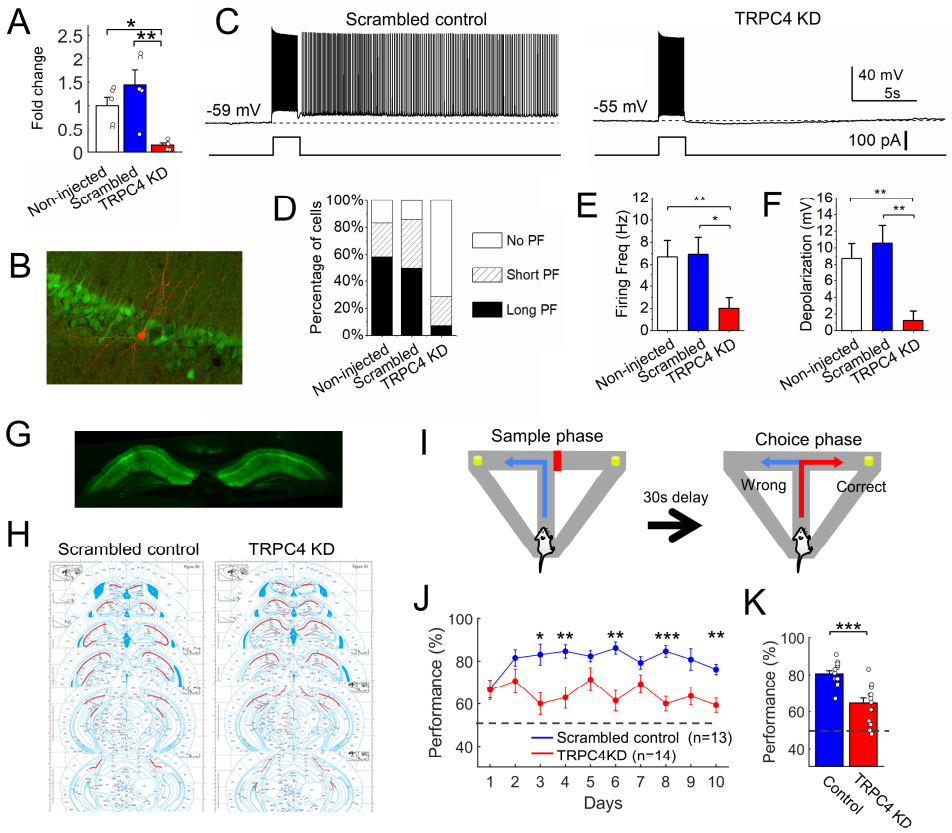

Figure 1. Hippocampal TRPC4 KD significantly reduces intrinsic persistent firing and impairs the delayed non-match-to-sample spatial working memory task (A) Reduced TRPC4 mRNA expression by the TRPC4 KD virus confirmed by RTq-PCR (one-way ANOVA, $p < 0.01$; Tukey post-hoc test corrected for multiple comparison, No virus vs Scrambled: $p = 0.33$, No virus vs TRPC4 KD: $p < 0.05$, Scrambled vs TRPC4 KD: $p < 0.01$; n = 5 in all groups). (B) An example hippocampal slice with GFP-expressing cells due to TRPC4 KD virus injection and a recorded neuron (red). (C) Persistent firing observed in a CA1 pyramidal cell infected with the scramble control virus (upper trace) and an absence of persistent firing in a cell infected with the TRPC4 KD virus (lower trace). The bottom trace indicates injected current. The red part of this trace corresponds to the 10 s interval when firing rate and depolarization were measured in E and F. (D) Percentages of cells responded with persistent firing (n = 12, 14 and 14, respectively; No PF: no persistent firing. Short PF: persistent firing which did not last for 30 s. Long PF: persistent firing lasted longer than 30 s). Fisher's exact test, Non-injected vs Scrambled: $p = 1$; Non-injected vs TRPC4 KD: $p = 0.0079$; Scrambled vs TRPC4 KD: $p = 0.0063$. (E and F) TRPC4 KD significantly decreased frequency of persistent firing and membrane depolarization measured during the 10 s period after the triggering stimulus (Frequency: Kruskal Wallis test, $p = 0.0023$, Chi-sq = 12.18, df = 2; Tukey post-hoc test, Non-injected vs Scrambled: $p = 0.99$, Non-injected vs TRPC4 KD: $p = 0.0077$, Scrambled vs TRPC4 KD: $p = 0.0074$; Depolarization: Kruskal–Wallis test, $p = 0.0116$, Chi-sq = 8.92, df = 2; Tukey post-hoc test, Non-injected vs Scrambled: $p = 0.89$, Non-injected vs TRPC4 KD: $p = 0.017$, Scrambled vs TRPC4 KD: $p = 0.047$; n = 12, 14 and 14, respectively). KD, knockdown; ANOVA, analysis of variance. (G) An example of hippocampal GFP expression after TRPC4 KD virus injection. (H) Summary of virus expression along the rostro-caudal axis from all mice. Red lines indicate the maximum extent of virus spread in each rostro-caudal plane. (I) The delayed non-match-to-sample spatial working memory task in a T-maze. (J) Working memory performance in scrambled control and TRPC4 KD group animals over ten days. Two-way ANOVA suggested significant main effects of the animal group ($p < 0.0001$). T-tests corrected for multiple comparisons suggested significant differences on days 3 ($p = 0.020$), 4 ($p = 0.0086$), 6 ($p = 0.0019$), 8 ($p < 0.001$), and 10 ($p = 0.0040$). (K) Averaged working memory performances of TRPC4 KD mice were significantly lower than the scrambled control group (T-test, $p < 0.001$; n = 13 and 14, respectively). KD, knockdown; ANOVA, analysis of variance.

101 around the delay period using the pre-delay period as the baseline in cells from the control and TRPC4

102 KD groups (Fig. 2B, see Methods). The cells were sorted based on their mean activity during the delay

103 period (0–25 s; orange line at the top of Fig. 2B). While a substantial portion of cells at the top of the

104 figure showed increased activity during the delay in the control group (top ~10%; Fig. 2B, left), such

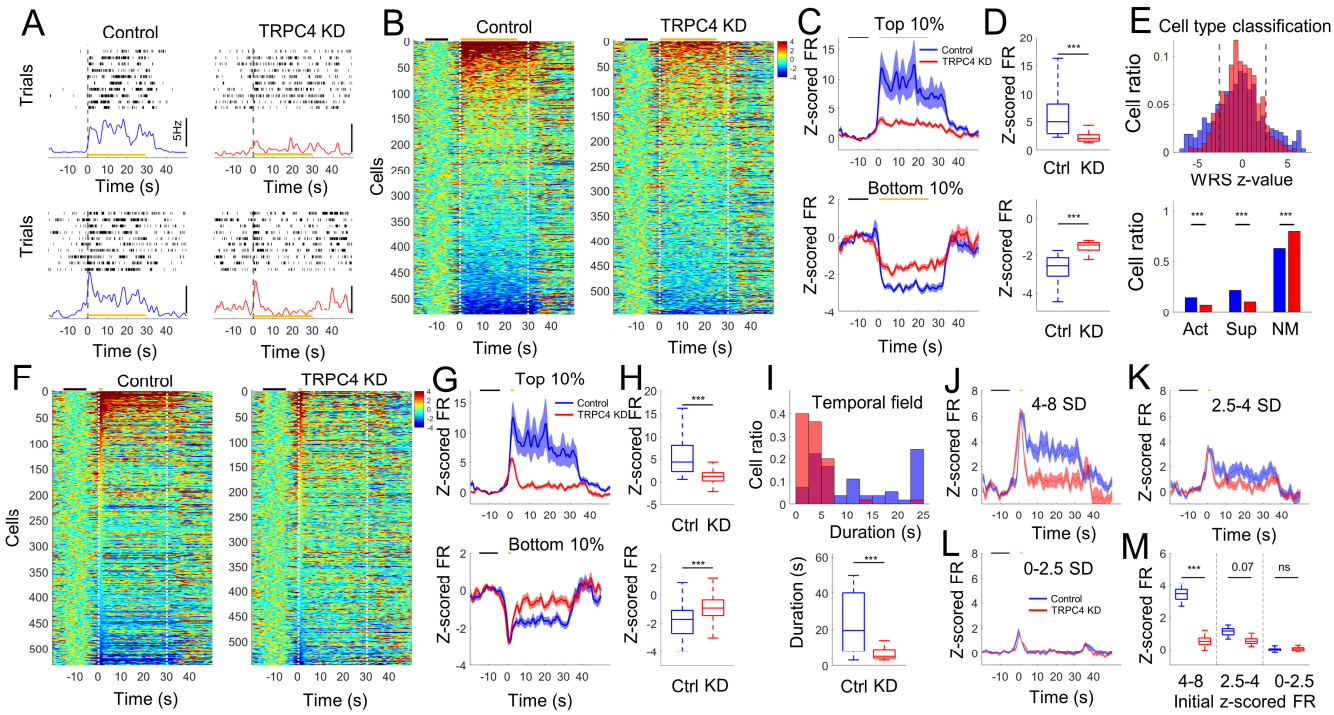

Figure 2. TRPC4 KD suppresses in vivo persistent activity (A) Example firing pattern (raster plot) and averaged firing rate (lower panel) of two cells from the control and TRPC4 KD groups around the delay period of the spatial working memory task. (B) Z-scored firing rate of all cells sorted by the delay period activity. Vertical dashed lines indicate the onset and offset of the delay period. Black and orange horizontal lines at the top of each panel indicate the baseline period and period for cell sorting, respectively. (C) Averaged z-scored firing rate (FR) of the top (upper panel) and bottom (lower panel) 10% cells in B. (D) Comparison of z-scored firing rate of the top (upper panel) and bottom (lower panel) 10 % cells in B averaged over the delay period (0–25 s) (WRS test, $p < 0.001$ and $p < 0.001$ for upper and lower panels respectively). (E) Classification of activated (Act), suppressed (Sup), and non-modulated (NM) cells using the Wilcoxon rank sum (WRS) test. The upper panel shows the distribution of WRS z-values, and the lower panel shows the ratio of cells in each category (Chi-square test, $p<0.001$ for all categories). (F) Z-scored firing rate of all cells sorted by the activity at the initial part of the delay period (0–2 s). Black and orange horizontal lines at the top of each panel indicate the baseline period and period for cell sorting, respectively. (G) Averaged z-scored firing rate of top (upper panel) and bottom (lower panel) 10% cells in F. (H) Comparison of z-scored firing rate of the top (upper panel) and bottom (lower panel) 10% cells in F averaged over the delay period (0–25 s) (WRS test, $p < 0.001$ and $p < 0.001$ for upper and lower panels respectively). (I) Distribution (upper panel) and comparison (lower panel) of temporal field duration among the top 10% cells (WRS test, $p < 0.001$). (J-L) Averaged z-scored firing rate of cells that showed 4-8 (J), 2.5-4 (K), and 0-2.5 (L) SD peak z-scored firing rate at the initial part of the delay (0-2 s). (M) Comparison of activity during the delay (4-25 s) period in cells that showed different levels of initial activation corresponding to J to L (WRS test, $p < 0.001$, $p = 0.07$, and $p = 0.58$ for J, K, and L, respectively). KD, knockdown

105 an increase was less prominent in the TRPC4 KD group (Fig. 2B, right). The activity of the top 10%
106 cells was significantly lower in the TRPC4 KD group (top panels in Fig. 2C and D). Similarly,
107 suppression of the bottom 10% cells in the TRPC4 KD group was significantly weaker (bottom panels
108 in Fig. 2C and D), indicating that both positive and negative modulations were compromised in the KD
109 group. Accordingly, TRPC4 KD significantly reduced the number of delay-activated (Act) and delay-
110 suppressed (Sup) cells and increased the number of non-modulated (NM) cells (Fig. 2E).

111 If intrinsic persistent firing was supporting *in vivo* persistent firing, TRPC4 KD should increase
112 transiently active cells. To test this, we sorted the cells using only activity during the first two seconds
113 of the delay period (0–2 s, Fig. 2F). The activity of initially active cells significantly decreased during
114 the delay period in the KD group, whereas more cells in the control group maintained their activity until
115 the end of the delay period (Fig. 2F and G). The activity measured during the entire delay period (0–25
116 s) was significantly lower in the KD group (Fig. 2H). We measured the temporal field duration to
117 quantify the duration of continuous elevation of the firing rate (Fig. 2I; see Methods). While the control
118 group showed a wide distribution of temporal field duration up to the full delay duration, the majority
119 of the TRPC4 KD group cells showed a temporal field shorter than 7.5 s (Fig. 2I, upper panel). The
120 mean temporal field duration was significantly shorter in the TRPC4 KD group (Fig. 2I, lower panel).
121 These data indicated that TRPC4 KD increased transient firing *in vivo,* as expected from our *in vitro*
122 results.

123 However, the initial activity of the top 10% cells was stronger in the control group (Fig. 2G,
124 upper panel), which could have resulted in stronger persistent firing in this group. To test this possibility,
125 we filtered cells based on their initial (0-2 s) activity levels (Fig. 2J-M). The control group cells with
126 initial activity increases of 4–8 and 2.5–4 standard deviations (SD) maintained a greater elevated level
127 of activity until the end of delay compared to KD group cells (Fig. 2J and K), whereas those with initial
128 activity of 0–2.5 SD did not show elevated activity (Fig. 2L). The sustained activity measured at 4–25
129 s was smaller in the KD group with 4–8 and 2.5–4 initial SD (Fig. 2M), indicating that the different
130 activities between the two groups are not simply due to the difference in initial activation. Thus, more

KD cells showed transient activity during the delay period, supporting the contribution of TRPC4 channels to sustained activity *in vivo* in a similar manner as *in vitro*.

Temporal sorting reveals reduced persistent firing in TRPC4 KD mice

We further characterized the effect of TRPC4 KD using temporal sorting[27,28]. For this analysis, we selected putative pyramidal cells active (firing rate > 2 Hz) in at least one bin during or near the delay period (see Methods, 196/533 control cells and 235/549 TRPC4 KD cells) and sorted them according to their activity peak time, as in previous reports[28] (Fig. 3A). We found an overrepresentation of the

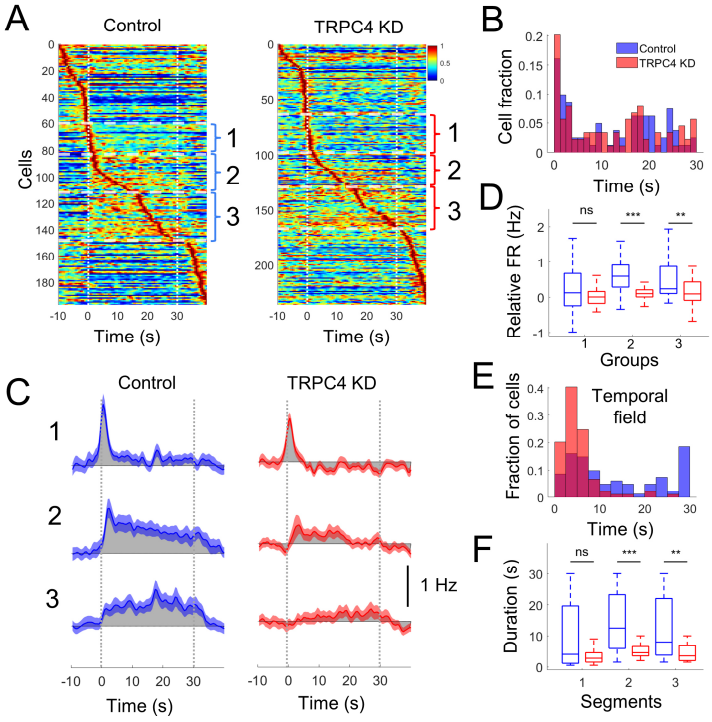

Figure. 3. Peak time sorting also shows reduced persistent activity in TRPC4 KD mice (A) Normalized firing rate of cells sorted by their peak times. Vertical dashed lines indicate the onset and offset of the delay period. Horizontal dashed lines and numbers (1-3) on the right of each panel indicate divisions of cells by their peak times (group 1: 0–2.5 s, group 2: 2.5–16.5 s, and group 3: 16.5–30 s). (B) Distribution of peak time of all cells within the delay period. Peak time distribution is not significantly affected by TRPC4 KD (WRS test, $p = 0.74$). (C) Averaged relative firing rate (compared to baseline firing rate) of cells belonging to each peak time segment shown in A. Gray shades indicate a difference from the baseline firing rate. Note, a prominent, long-lasting elevated firing rate in control cells in groups 2 and 3. (D) Relative firing rate (FR) measured during the delay (0 to 30 s) compared to the baseline period in cells in each peak time segment. (E) Distribution of temporal field duration of all cells peaked during the delay period (group 1-3) (WRS test, $p < 0.001$). (F) Comparison of the duration of the field in each group (WRS test, $p = 0.32$, $p < 0.001$, and $p = 0.006$ for groups 1, 2, and 3, respectively). KD, knockdown

138 initial part of the delay period (0–3 s) in both the control and TRPC4 KD group (Fig. 3B). However,
139 TRPC4 KD did not significantly alter peak time distribution.

140 To evaluate potential effects of TRPC4 KD on cells with different peak times, cells were
141 separated into three groups based on their peak times during the delay (Fig. 3A). While cells that peaked
142 at 0–2.5 s (group 1) showed transient peak activity, the other two groups that peaked later in the delay
143 (2.5–16.5 s: group 2, 16.5–30 s: group 3) exhibited, on average, an elevated firing rate throughout the
144 delay period in the control group (Fig. 3C left). While TRPC4 KD did not affect the transient activation
145 of cells at the initial part of the delay (group 1), it reduced long-lasting elevated firing of group 2 and 3
146 cells (Fig. 3C, right). Accordingly, the firing rate averaged over the delay period was significantly lower
147 in groups 2 and 3 of the KD group but not in group 1 (Fig. 3D). Combining all cells that peaked during
148 the delay, the KD group had more cells with shorter fields (See Methods; Fig. 3E). The duration of the
149 field from the KD group cells was significantly shorter in groups 2 and 3 (Fig. 3F). The specific effect
150 of TRPC4 KD on cells with longer temporal fields, further support the idea that the ability of single
151 neurons to sustain firing is necessary specifically for persistent firing *in vivo*.

152

153 **Activity outside the delay period is intact**

154 To further assess whether the effect of TRPC4 KD was specific to the delay period, we compared the
155 activity of cells at different time points, ranging from 4 s before delay onset to 3 s after the delay (Fig.
156 4). First, cells were sorted using the z-scored activity of each cell at 3 to 4 s before the start of the delay
157 period (-4 to -3 s; Fig. 4A), and the average activity of the top 10% cells from the control and KD groups
158 was compared (Fig. 4D most left). These cells were only temporarily active and did not display
159 persistent firing in either group, indicating that persistent firing was not ubiquitous. Neither activity of
160 the top 10 % cells during this 1 s window (-4 s in Fig. 4E) nor during the entire delay period (-4 s in
161 Fig. 4F) differed between the control and KD groups, indicating that TRPC4 KD did not have a strong
162 effect before the delay. Similar results were obtained 2 s before delay onset (-2 to -1 s; Fig. 4D, second
163 from left; Time -2 s in Fig. 4E and F). In contrast, control group cells activated during the delay (0-1,
164 10-11 and 20-21 s) showed stronger activity than KD cells, both during these 1s windows and during
165 the entire delay (Fig. 4B; Fig. 4D middle three panels; Time 0, 10, and 20 s in Fig. 4E and F). Finally,

when active cells were detected after the delay period (1-2 and 3-4 s later; Fig. 4C; Fig. 4D, two rightmost panels), the activity of these cells was transient and similar between the two groups (Time 1 and 3 s in Fig. 4E and F). This suggests that persistent firing does not occur before or after the delay period, and that TRPC4 KD specifically affects the activity of neurons during the delay period, as opposed to worsening the signal-to-noise ratio throughout the task.

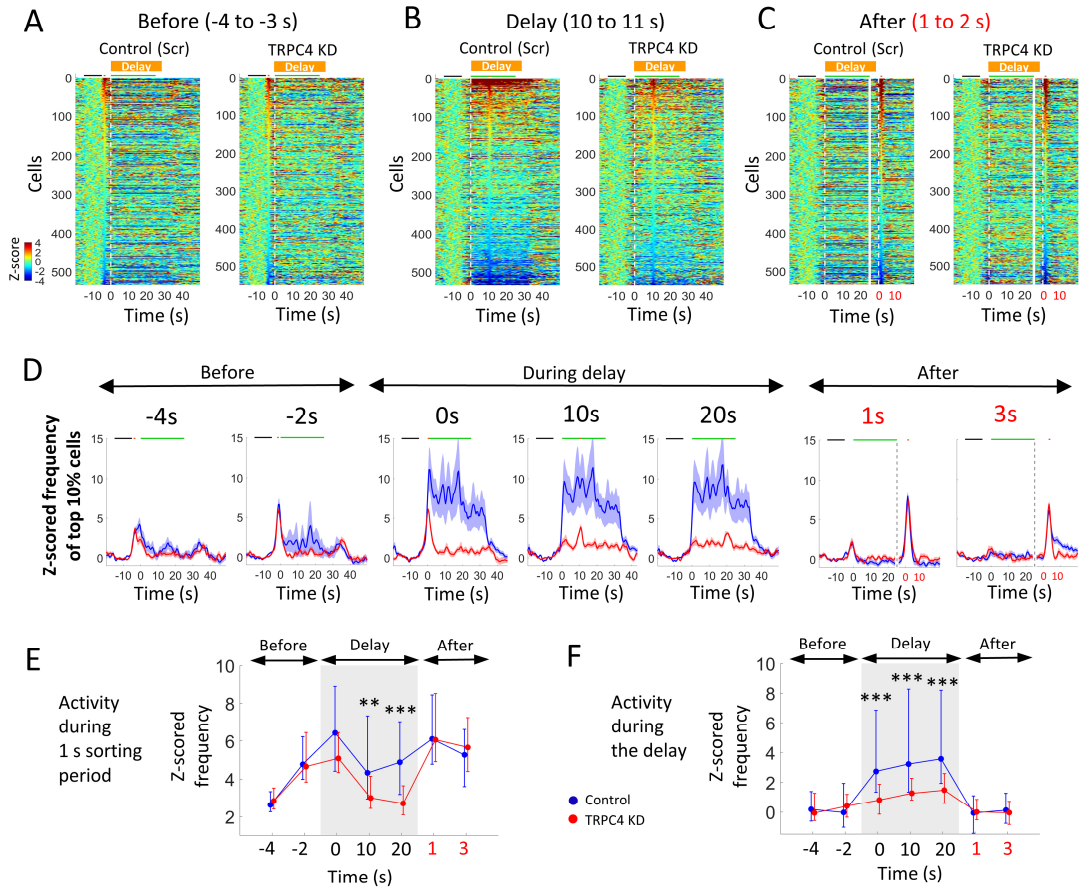

Figure 4. Activity outside the delay period is not strongly affected by TRPC4 KD (A-C) Z-scored firing rate of all cells sorted by their activity during the (A) 4 to 3 s before delay, (B) 10 to 11 s from the start of delay, and (C) 1 to 2 s after the delay offset. Vertical dashed lines indicate the onset and offset of the delay period. Black, orange, and green horizontal lines at the top of each panel indicate the baseline period, period for cell sorting, and period for delay activity measurement, respectively. In C, the white solid vertical line indicates the separation of the color plot into two parts that are aligned to the delay onset (left of the line) and offset (right of the line). (D) Averaged z-scored firing rate of the top 10% cells at different time points. Note that the cells chosen for each panel are therefore different. The vertical dotted lines in the two last panels correspond to the time when data alignment changed as in C. (E) Comparison of z-scored firing rate of the top 10 % cells measured specifically during the one second-long sorting period (corresponding to the orange horizontal lines in D; Ranksum test with Bonferroni correction, p = 0.31, 1.45, 0.29, 0.003, < 0.001, 1.45, 0.28, respectively). (F) Comparison of z-scored firing rate of the top 10 % cells measured specifically during the delay period (corresponding to the green horizontal lines in D; Ranksum test with Bonferroni correction, p = 0.88, 1.46, < 0.001, < 0.001, < 0.001, 1.47, 1.10, respectively). Data points show the median, and error bars indicate the upper and lower quartiles. KD, knockdown

171

172 **Activity of putative pyramidal cells and interneurons**

173 We next investigated whether the difference in the delay period activity between control and TRPC4
174 KD mice was cell type-dependent. We separated recorded neurons into putative pyramidal neurons and
175 interneurons based on their average firing rates and spike durations (see Methods). Putative pyramidal
176 cells in the control group showed strong activity during the delay, with TRPC4 KD suppressing this
177 activity (Extended Data Fig. 1A-D). On the other hand, the activity of the top 10% putative interneurons
178 during the delay period did not differ between the control and TRPC4 KD groups (Extended Data Fig.
179 1E-H). This suggests that putative interneurons are not the main source of the observed TRPC4 KD-
180 dependent changes.

181

182 **Information coded by persistent firing**

183 Next, we investigated the nature of information coded by cells with strong persistent firing during the
184 delay period. The hippocampus may support spatial working memory in at least two ways. First,
185 persistent firing may sustain working memory content (e.g., turn direction in the sample trial) during
186 the delay period[24,25]. Second, the hippocampus may support spatial working memory tasks by providing
187 information of the current spatial location[29,30]. However, whether the long-lasting persistent firing codes
188 for the turn direction or current spatial information remains unclear.

189 We first compared the activity of cells in the control group during the delay period with that
190 during the inter-trial interval (ITI; Extended Data Fig. 2A). Since the animals were in the same start
191 area in both the delay period and ITI, the different activities in these phases may suggest the coding of
192 task-relevant information. Cells were sorted according to their activity during the delay period
193 (Extended Data Fig. 2B). Control cells highly active during the delay period were strongly active during
194 ITI as well, without significant difference, as shown in Extended Data Fig. 2B and C. The activity of
195 individual cells during the delay period was similar to that during ITI, as shown in Extended Data Fig.
196 2D.

197 We further used a support vector machine (SVM) to test whether it could be trained to predict
198 the delay and ITI phases based on the activity of all cells in each recording session (control: n = 16,

199 TRPC4 KD: n = 18 sessions; see Methods for details; Extended Data Fig. 2E and F). SVM could not
200 differentiate the delay vs. ITI phases in any of the recordings (Z-values were lower than 1.96) from the
201 control and TRPC KD groups. Furthermore, there were no differences between the control and KD
202 groups. Together, these findings contradicted the idea that persistent firing codes for task-phase-relevant
203 information.

204 Second, we asked whether the direction of the past or future turns was coded in persistent
205 activity observed during the delay period. We sorted cells from the control group using the delay activity
206 of the left trials (left turn on the sample trial; Extended Data Fig. 2G, left) and used the same order for
207 the delay activity of the right trials (Extended Data Fig. 2G, right). A small but significant difference
208 was observed when comparing the activity of the top 10% cells (Extended Data Fig. 2H). The activity
209 of individual cells in the left and right delay periods was generally similar but showed more differences
210 than the comparison between the ITI and delay phases (Extended Data Fig. 2I). While this difference
211 between the left and right delay activity indicates the potential existence of coding of the turn direction,
212 random noise may result in such differences.

213 Therefore, we further used an SVM to test whether the population activity codes for the left vs.
214 right turn in each recording session (control, n = 15; TRPC4 KD, n = 14). SVM prediction accuracy
215 exceeded 70% in most of the sessions (Extended Data Fig. 2J) just before the onset of the delay period
216 (-3 to 0 s), when the animal was still in the return arm of the T-maze, and this prediction accuracy was
217 significantly higher than the chance level in approximately half (53.3%) of the sessions (Extended Data
218 Fig. 2K). However, prediction performance decreased quickly as the delay started (0–3 s; Extended
219 Data Fig. 2J and K), and almost none of the sessions reached a significant level in either the control or
220 TRPC KD group after 3 s (3–25 s) in the delay period. No difference was observed between the SVM
221 performance of the control and KD groups for any of the three time-segments.

222 We further asked whether the delay period activity codes for the future turn direction
223 (prospective coding) rather than the past turn direction from the sample phase (retrospective coding).
224 The SVM prediction for prospective coding was tested using the activity from the 3-25 s period during
225 the delay of all or only correct trials (Extended Data Fig. 2L and M). Most of the session did not reach
226 significant levels both in the control and KD group and there was no difference between the control and

227 KD. Together, these suggest that coding for the direction of turns during the delay period is weak. These
228 agree with recent publications which pointed out that hippocampal delay period activity does not[31] or
229 only weakly[32] codes for the direction of the past or future turns.
230
231 **Persistently active cells encode spatial information**
232 Next, we tested the hypothesis that persistently active cells primarily code for spatial information.
233 Computational models of hippocampal place cells suggest that spatial representation is maintained by
234 the self-sustained activity of a subset of place cells[33]; therefore, persistent firing might be involved in
235 the maintenance of spatial representation. We first sorted cells in order of the strength of persistent
236 firing during the delay period as in the previous sections (Fig. 5A). We then calculated the spatial
237 information of each cell using the entire duration of the recording, including the sample and choice
238 phases from all 10 trials (Fig. 5B). Spatial information was particularly high in the control group cells
239 which showed strong persistent firing (blue line, Fig. 5B). Spatial information of the top 10% cells in
240 Fig. 5A was significantly lower in the KD group compared to the control group (Fig. 5C), whereas that
241 of the bottom 10% cells was significantly higher in the KD group (Fig. 5D).
242 We visualized the spatial rate maps of the top 10% cells in control and TRPC4 KD groups (Fig.
243 5E and F). While the control group cells generally showed a clear field within the start area, fields of
244 TRPC4 KD cells were less confined often having multiple fields outside the start area (Fig. 5E and F).
245 The averaged rate map from top 10% control cells showed a distinct firing at the start area, while that
246 from the KD cells showed spatially less defined activity (Fig. 5G and H). This suggests that cells with
247 strong persistent firing during the delay period are those with better-defined place fields in the start area
248 and consequently have higher spatial information. This suggests that TRPC4 KD destabilized spatial
249 representation by preventing persistent activity of CA1 place cells while the animal remained in the
250 start area.
251
252 **Selective decrease of spatial information in start and goal areas**

253 In the T-maze task, in addition to the start area, the animals stayed for an extended period in the goal

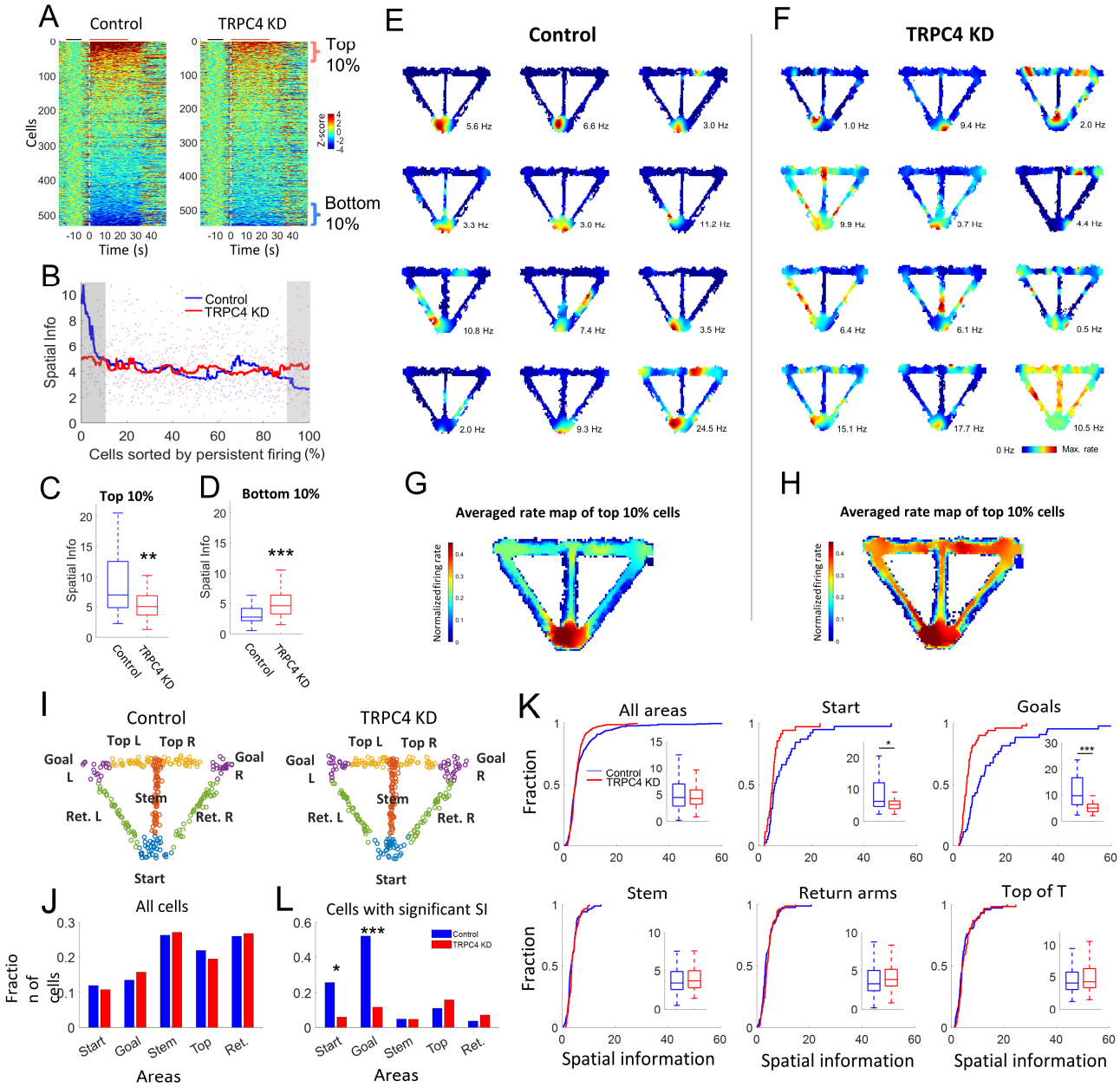

Figure 5. TRPC4 supports persistent activity of spatial cells when animals stay in a place for an extended duration (A) Z-scored firing rate of all cells sorted by the averaged activity during the delay period (0–25 s), as in Fig. 2B. Vertical dashed lines indicate the onset of the delay period. (B) Spatial information of all cells plotted in the order of the sorting in A. Solid lines indicate the moving average. Red and blue shaded areas indicate the top and bottom 10% cells. (C and D) Comparison of spatial information between the control and TRPC4 KD groups in the top (C; WRS test, $p = 0.0024$; $n = 53$) and bottom (D; WRS test, $p < 0.001$; $n = 55$) 10% cells. (E and F) Example spatial rate maps of the top 10% cells in control (E) and TRPC4 KD (F) groups. The maximum firing rate of each cell is indicated at the bottom right corner of each panel. (G and H) Averaged spatial rate maps of all top 10 % cells in the control (G) and TRPC4 KD (F) groups. (I) Distribution of peak firing location of all putative pyramidal cells on the T-maze. Each circle corresponds to a cell, and colors indicate different sub-areas. Top: top of the T-maze, Ret.: return arm, L: Left, R: Right. (J) Fractions of cells classified into each sub-area. (K) Distribution of spatial information of cells in all and each sub-area. Insets are comparisons of spatial information between the control and KD cells (WRS test, All areas: $p = 0.56$, Start: $p < 0.019$, Goals: $p < 0.001$, Stem: $p = 0.41$, Return arms: $p = 0.19$, and Top of T: 0.35). (L) Number of place cells with significant spatial information in each sub-area (Fisher's exact test, $p = 0.027$, < 0.001, 1, 0.45, and 0.49, respectively, from left to right). KD, knockdown

254 areas where they consumed their rewards, whereas they run through other subareas of the maze (e.g.,
255 stem, return arm). If intrinsic persistent firing supports continuous place cell activity, TRPC4 KD might
256 have affected spatial representation specifically in the start and goal areas without affecting that in other
257 subareas. To test this, we first detected the location of firing fields within the T-maze for each putative
258 pyramidal cell (see Methods). Next, we divided cells into different groups depending on the subareas
259 of the T-maze where the location of field centers fell (Fig. 5I). The number of cells in each subarea was
260 similar in the control and KD groups (Fig. 5J).

261 We then compared the spatial information of the cells in each subarea (Fig. 5K). Spatial
262 information was slightly smaller in the TRPC4 KD group when all subareas were combined (all areas),
263 without a significant difference. Consistent with previous observations, the spatial information of the
264 cells in the start area was significantly lower in the KD group. Interestingly, a similar difference was
265 observed in the goal area, where the animals stayed for an extended time. However, spatial information
266 was not significantly different in other areas, such as the stem, return arms, and top of the T. Morefover,
267 the number of place cells (cells significantly modulated by location) was higher in the control group
268 than in the KD group only in the start and goal areas (Fig. 5L). These results suggest that TRPC4 KD
269 selectively impairs the spatial representation of cells when animals stay in a place, and place cells need
270 to fire persistently. This is in line with the time-domain analysis (Fig. 4), which revealed a specific
271 effect of TRPC4 KD on cellular activity during, but not before or after, the delay. In addition, the
272 compromised spatial representation observed in the start and goal areas in TRPC4 KD animals is not
273 associated with a lower running speed or weaker theta oscillations (Extended Data Fig. 3).

274

275 **Gradual decrease of left and right goal representation**

276 We further analyzed cellular activity and spatial representation in the goal areas (Fig. 6) since the
277 encoding of left vs. right goals in the hippocampus during the sample phase may be crucial for task
278 performance[30]. First, we tested whether persistent activity differed in the goal areas. We limited our
279 analysis to trials in which animals spent at least 10 s continuously within the goal area (see Methods for
280 details). Fig. 6A shows the z-scored firing rate of all cells where the time 0–10 s corresponds to the 10
281 s period when animals continuously stayed in the left goal area in the sample phases (indicated by the

orange line on the top). Activity of the top 10% cells was significantly lower in the TRPC4 KD group, both in the left and right goals (Fig. 6B and C). These results indicated that TRPC4 KD reduced the continuous activity of cells in the goal area as in the start area.

Next, we investigated whether this affected the representations of the left and right goals at the population level using an SVM (Fig. 6D and E). This analysis was conducted using the activity of all cells from the 10 s goal period in each recording session with a minimum of 15 cells (n = 15 and 14

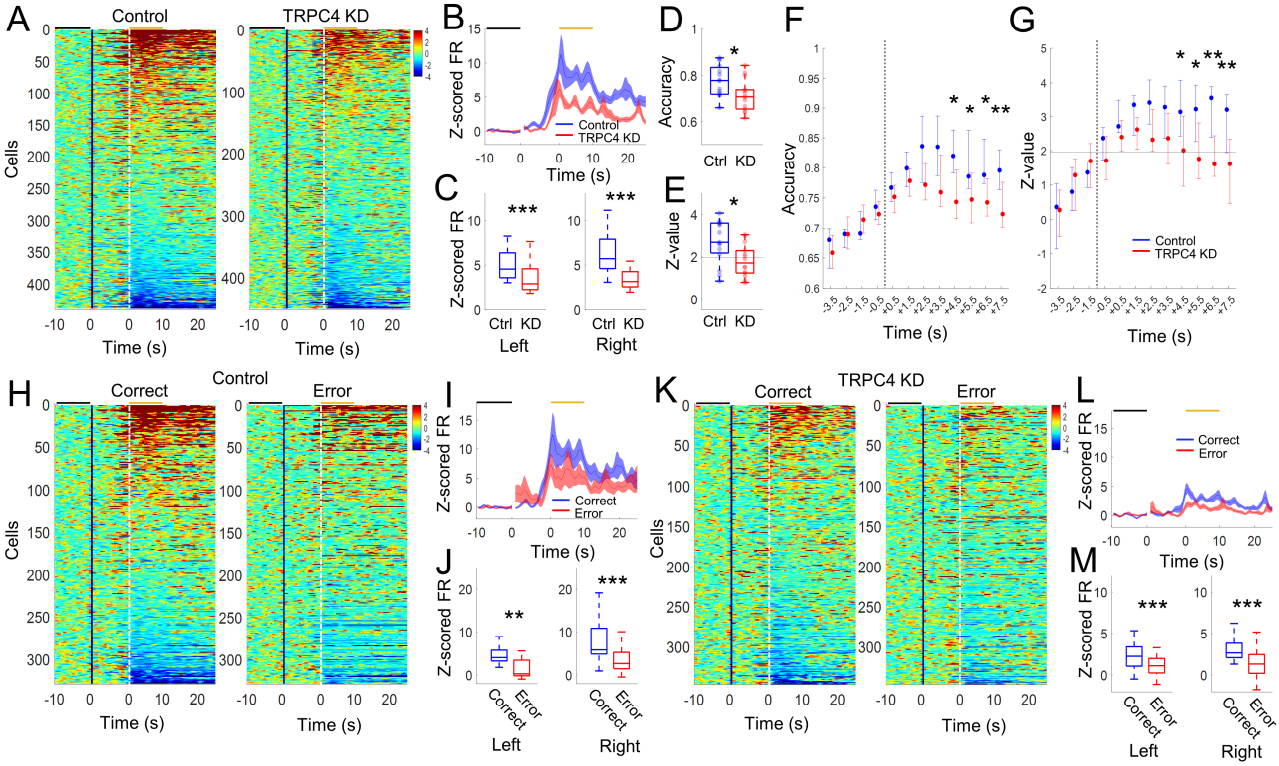

Figure 6. Gradual decrease of spatial representation in the goal areas may have resulted in the poor task performance of TRPC4 KD mice (A) Z-scored firing rate of cells sorted by their activity during the 10 s goal period when animals continuously stayed in the left goal area. The black vertical gap separates the first 10 s, which is referenced to the end of the ITI period, and the rest, which is referenced to the start of the goal entry. The black and orange horizontal lines on the top indicate the baseline and 10 s goal period, respectively. (B) Activity of the top 10% cells in A. (C) Comparisons of activity of the top 10% cells during the 10 s goal period (0-10 s) at the left and right goals (WRS test, $p < 0.001$ and $p < 0.001$, respectively). (D-E) Accuracy (D) and z-value (E) from the SVM prediction of left vs right goals based on the activity of all cells in individual sessions during the 10 s goal period (WRS test, $p = 0.019$ and 0.017 in D and E, respectively). The horizontal line in E indicates a 5% significance level. (F-G) Accuracy (F) and z-value (G) from the SVM prediction of left vs right goals at different time periods before and during the 10 s goal period. The vertical dotted lines indicate goal entry, and the horizontal line in G indicates 5% significance level. (H) Z-scored firing rate of cells from the control group animals sorted by their combined sort order (see text) during the 10 s goal period in the left goal area from the correct (left panel) and error (right panel) trials. (I) Activity of the top 10% cells in H. (J) Comparisons of activity of the top 10% cells during the 10 s goal period (0-10 s) from correct (blue) and error (red) trials at the left and right goals (WRS test, $p = 0.0018$ and < 0.001, respectively). (K-M) Same as panels H to J but for the TRPC4 KD group (WRS test, $p < 0.001$ and < 0.001, for left and right trials, respectively in M). KD, knockdown

288 sessions in the control and KD groups, respectively). The left vs. right goal prediction accuracy and z-
289 values of the SVM analysis were significantly lower in the TRPC4 KD group (Fig. 6D and E). While
290 80.0% of sessions had significantly higher prediction accuracy than chance level in control, only 42.8%
291 were significantly higher than chance level in the KD group (Fig. 6E), suggesting that representations
292 of left vs. right goals may have been compromised in the TRPC4 KD group.

293 We further investigated whether a gradual decline in left and right goal representation may be
294 detected over time within the 10 s goal period owing to the lack of persistent activity in the TRPC4 KD
295 group (Fig. 6F and G). We performed a similar SVM analysis at different time points starting from the
296 pre-goal period (-3.5 s) using a sliding (1 s) 5 s window (time indicated in Fig. 6F and G is the center
297 of the window). The prediction accuracy increased over time as the animal approached the goal area (-
298 3.5 to +1.5 s, note that +1.5 still includes 3 s of pre-goal time). Importantly, the prediction accuracy and
299 z-value between the control and KD groups differed starting at +4.5 s into the goal area (Fig. 6F and
300 G), indicating a faster decline in goal representation in the KD group. These suggest the specific role of
301 TRPC4 KD on the maintenance of spatial representation.

302

303 **Behavioral relevance**

304 Finally, we asked whether the activity of the cells in the goal differed between correct and incorrect
305 trials, using recording sessions with at least two error trials. The activity of the cells was first averaged
306 over all trials, including both correct and error trials, to obtain combined sorting order. Subsequently,
307 the activity profiles from correct and incorrect trials were separately averaged for each cell and sorted
308 by the combined sort order (Fig. 6H). Persistent firing of the top 10% cells was significantly lower in
309 the error trials compared to the correct trials in the control group for both the left and the right goals
310 (Fig. 6I and J). Similar differences were observed in the KD group (Fig. 6K-M). These results are
311 consistent with the idea that hippocampal goal activity during the sample phases contributes to task
312 performance[30,34]. Together, our data suggested that the intrinsic mechanism of persistent firing supports
313 a stable spatial representation of goal locations, which is necessary for correct encoding of left vs right
314 turns.

315

316 # Discussion

317 Despite empirical evidence[7,10,11,35] and theoretical supports[15–17], it remained unclear whether individual
318 cells support persistent activity *in vivo*. We identified the TRPC4 channel as a molecular mechanism of
319 intrinsic persistent firing in CA1 pyramidal cells[23] and demonstrated that persistent firing was
320 significantly reduced *in vivo* in a spatial working memory task by TRPC4 KD (Fig. 2-3). These results
321 provide the first direct evidence that a single-cell mechanism supports persistent firing *in vivo* during a
322 cognitive task. Further analyses revealed a specific effect of TRPC4 KD on persistently firing (Fig. 4
323 and 5) without disrupting signal-to-noise ratio in general. The behavioral outcome align with studies
324 indicating the role of TRPC channels[36,37] and manipulations that potentially disrupt persistent firing[21]
325 in working memory.

326 Classically, persistent firing during the delay period has been believed to hold working memory
327 content. Abundant evidence supports this in the prefrontal cortex and hippocampus during the working
328 memory delay period in humans and monkeys[26,38] whereas data in rodents remains mixed[31,32,39]. In
329 agreement with these rodent studies, our SVM analyses suggest the absence or very weak presence of
330 working memory content in the delay phase (Extended Data Fig. 2). An alternative theory posits that
331 the hippocampus contributes to this type of working memory task by providing spatial information
332 during the sample phase to help encoding, rather than maintaining working memory content[30,40,41]. We
333 found that neurons with strong persistent firing had larger spatial information, and TRPC4 KD reduced
334 spatial information specifically in places where persistent firing was observed (start and goal areas),
335 suggesting that persistent firing mainly codes for spatial information (Fig. 5).

336 Hippocampal place cells are believed to be supported by path integration, which requires the
337 maintenance and continuous updating of spatial representation[33]. Computational studies have suggested
338 that similar attractor networks, such as continuous attractor networks, support working memory and
339 path integration[42,43]. The continuous attractor model maintains spatial representation by persistent firing
340 of a subset of neurons, "bump of activity", through recurrent synaptic networks[43]. However, the neural
341 networks of CA1, where place cells were most intensively studied, and MEC layer II, where grid cells

were found, lack recurrent excitatory networks[44,45]. Additionally, these network models are sensitive to distractors, whereas experimental evidence suggests their robustness to distractors[46,47].

Including the intrinsic cellular mechanisms of persistent firing in attractor networks has been shown to ameliorate these problems increasing stability against noise, reducing drift, and reducing sensitivity to parameters[17,18,48] . Upon empirically disrupting the intrinsic mechanism of persistent firing *in vivo*, we observed that spatial representation was compromised specifically at the start and goal areas. The intactness of spatial representation in other areas suggests that attractor dynamics were not completely absent, in agreement with the hybrid model. The gradual degradation of goal representation (Fig. 6) suggests a drift that can be predicted from the loss of intrinsic properties in the hybrid model[17].

An intact spatial representation outside the start and goal areas can be supported by external cue-based navigation[49] that may not require information retention by persistent firing. Distal cues on the surrounding curtains and walls were visible to animals when they were in long corridors such as the stem and return arms, which was not the case in the start and goal areas. Alternatively, this could be attributed to the time required for persistent firing initiation, owing to the Ca2+-dependent biochemical processes involved in activating TRPC channels[13]. When the mice ran through the T-maze arms at a relatively high speed, the resulting short period of activation of each place cell may not have been long enough to fully activate the TRPC channels. Further studies are needed to clarify the exact mechanisms TRPC4 supports spatial representation in specific areas.

The prevailing view that neurons fire only when they receive sufficient input dictates current understanding of neural computation in the brain. Our findings challenge this view, revealing them as active contributors to information retention *in vivo*. This intrinsic persistent firing depends on the cholinergic system, which degrades in aging and Alzheimer's disease[50,51] causing cognitive impairments [52,53]. Our findings thus potentially reshape our general understanding of brain computation and highlights novel therapeutic targets for cognitive disorders.

References

1. Compte, A. Computational and in vitro studies of persistent activity: edging towards cellular and synaptic mechanisms of working memory. *Neuroscience* **139**, 135–151 (2006).
2. Issa, J. B., Tocker, G., Hasselmo, M. E., Heys, J. G. & Dombeck, D. A. Navigating Through Time: A Spatial Navigation Perspective on How the Brain May Encode Time. *Annu Rev Neurosci* **43**, 73–93 (2020).
3. Major, G. & Tank, D. Persistent neural activity: prevalence and mechanisms. *Curr Opin Neurobiol* **14**, 675–684 (2004).
4. Zylberberg, J. & Strowbridge, B. W. Mechanisms of Persistent Activity in Cortical Circuits: Possible Neural Substrates for Working Memory. *Annu. Rev. Neurosci.* **40**, 603–627 (2017).
5. Forbes, A. *Physiology of the Nervous System* . By J. F. Fulton. London, New York, Toronto: Oxford University Press, 1938. Pp. xv + 675. *Science* **90**, 17–18 (1939).
6. Hebb, D. O. *The Organization of Behavior; a Neuropsychological Theory*. xix, 335 (Wiley, Oxford, England, 1949).
7. Andrade, R. Cell excitation enhances muscarinic cholinergic responses in rat association cortex. *Brain Research* **548**, 81–93 (1991).
8. Fraser, D. D. & MacVicar, B. A. Cholinergic-Dependent Plateau Potential in Hippocampal CA1 Pyramidal Neurons. *J. Neurosci.* **16**, 4113–4128 (1996).
9. Klink, R. & Alonso, A. Muscarinic Modulation of the Oscillatory and Repetitive Firing Properties of Entorhinal Cortex Layer II Neurons. *Journal of Neurophysiology* **77**, 1813–1828 (1997).
10. Krnjević, K., Pumain, R. & Renaud, L. The mechanism of excitation by acetylcholine in the cerebral cortex. *J Physiol* **215**, 247–268 (1971).
11. Egorov, A. V., Hamam, B. N., Fransén, E., Hasselmo, M. E. & Alonso, A. A. Graded persistent activity in entorhinal cortex neurons. *Nature* **420**, 173–178 (2002).
12. Hasselmo, M. E. & Sarter, M. Modes and models of forebrain cholinergic neuromodulation of cognition. *Neuropsychopharmacology* **36**, 52–73 (2011).
13. Knauer, B., Jochems, A., Valero-Aracama, M. J. & Yoshida, M. Long-lasting intrinsic persistent firing in rat CA1 pyramidal cells: a possible mechanism for active maintenance of memory. *Hippocampus* **23**, 820–831 (2013).
14. Reboreda, A. *et al.* Do TRPC channels support working memory? Comparing modulations of TRPC channels and working memory through G-protein coupled receptors and neuromodulators. *Behav Brain Res* **354**, 64–83 (2018).
15. Fransen, E., Alonso, A. A. & Hasselmo, M. E. Simulations of the role of the muscarinic-activated calcium-sensitive nonspecific cation current INCM in entorhinal neuronal activity during delayed matching tasks. *J Neurosci* **22**, 1081–1097 (2002).
16. Hasselmo, M. E. Grid cell mechanisms and function: contributions of entorhinal persistent spiking and phase resetting. *Hippocampus* **18**, 1213–1229 (2008).
17. Camperi, M. & Wang, X. J. A model of visuospatial working memory in prefrontal cortex: recurrent network and cellular bistability. *J Comput Neurosci* **5**, 383–405 (1998).
18. Fall, C. P. & Rinzel, J. An intracellular Ca2+ subsystem as a biologically plausible source of intrinsic conditional bistability in a network model of working memory. *J Comput Neurosci* **20**, 97–107 (2006).
19. Goldman, M. S., Levine, J. H., Major, G., Tank, D. W. & Seung, H. S. Robust persistent neural activity in a model integrator with multiple hysteretic dendrites per neuron. *Cereb Cortex* **13**, 1185–1195 (2003).
20. Lin, C., Sherathiya, V. N., Oh, M. M. & Disterhoft, J. F. Persistent firing in LEC III neurons is differentially modulated by learning and aging. *Elife* **9**, e56816 (2020).

21. Glasgow, S. D. *et al.* Acetylcholine synergizes with netrin-1 to drive persistent firing in the entorhinal cortex. *Cell Reports* **43**, 113812 (2024).
22. Saber Marouf, B. *et al.* TRPC4 Channel Knockdown in the Hippocampal CA1 Region Impairs Modulation of Beta Oscillations in Novel Context. *Biology (Basel)* **12**, 629 (2023).
23. Arboit, A., Reboreda, A. & Yoshida, M. Involvement of TRPC4 and 5 Channels in Persistent Firing in Hippocampal CA1 Pyramidal Cells. *Cells* **9**, 365 (2020).
24. Olton, D. S., Becker, J. T. & Handelmann, G. E. Hippocampus, space, and memory. *Behavioral and Brain Sciences* **2**, 313–365 (1979).
25. Goldman-Rakic, P. S. Cellular basis of working memory. *Neuron* **14**, 477–485 (1995).
26. Kamiński, J. *et al.* Persistently active neurons in human medial frontal and medial temporal lobe support working memory. *Nat Neurosci* **20**, 590–601 (2017).
27. MacDonald, C. J., Lepage, K. Q., Eden, U. T. & Eichenbaum, H. Hippocampal 'time cells' bridge the gap in memory for discontiguous events. *Neuron* **71**, 737–749 (2011).
28. Pastalkova, E., Itskov, V., Amarasingham, A. & Buzsáki, G. Internally generated cell assembly sequences in the rat hippocampus. *Science* **321**, 1322–1327 (2008).
29. Nadel, L. & MacDonald, L. Hippocampus: cognitive map or working memory? *Behavioral and Neural Biology* **29**, 405–409 (1980).
30. Spellman, T. *et al.* Hippocampal-prefrontal input supports spatial encoding in working memory. *Nature* **522**, 309–314 (2015).
31. Sabariego, M. *et al.* Time Cells in the Hippocampus Are Neither Dependent on Medial Entorhinal Cortex Inputs nor Necessary for Spatial Working Memory. *Neuron* **102**, 1235-1248.e5 (2019).
32. Athanasiadis, M. *et al.* Low rate hippocampal delay period activity encodes behavioral experience. *Hippocampus* **34**, 422–437 (2024).
33. McNaughton, B. L., Battaglia, F. P., Jensen, O., Moser, E. I. & Moser, M.-B. Path integration and the neural basis of the 'cognitive map'. *Nat Rev Neurosci* **7**, 663–678 (2006).
34. Quirk, C. R. *et al.* Precisely timed theta oscillations are selectively required during the encoding phase of memory. *Nat Neurosci* **24**, 1614–1627 (2021).
35. Loewenstein, Y. *et al.* Bistability of cerebellar Purkinje cells modulated by sensory stimulation. *Nat Neurosci* **8**, 202–211 (2005).
36. Bröker-Lai, J. *et al.* Heteromeric channels formed by TRPC1, TRPC4 and TRPC5 define hippocampal synaptic transmission and working memory. *EMBO J* **36**, 2770–2789 (2017).
37. Lepannetier, S. *et al.* Activation of TRPC1 Channel by Metabotropic Glutamate Receptor mGluR5 Modulates Synaptic Plasticity and Spatial Working Memory. *Front Cell Neurosci* **12**, 318 (2018).
38. Fuster, J. M. Unit activity in prefrontal cortex during delayed-response performance: neuronal correlates of transient memory. *J Neurophysiol* **36**, 61–78 (1973).
39. Vogel, P., Hahn, J., Duvarci, S. & Sigurdsson, T. Prefrontal pyramidal neurons are critical for all phases of working memory. *Cell Rep* **39**, 110659 (2022).
40. Leis, T., Pallage, V., Toniolo, G. & Will, B. Working memory theory of hippocampal function needs qualification. *Behavioral and Neural Biology* **42**, 140–157 (1984).
41. Cacucci, F., Yi, M., Wills, T. J., Chapman, P. & O'Keefe, J. Place cell firing correlates with memory deficits and amyloid plaque burden in Tg2576 Alzheimer mouse model. *Proc Natl Acad Sci U S A* **105**, 7863–7868 (2008).
42. Durstewitz, D., Seamans, J. K. & Sejnowski, T. J. Neurocomputational models of working memory. *Nat Neurosci* **3**, 1184–1191 (2000).
43. Khona, M. & Fiete, I. R. Attractor and integrator networks in the brain. *Nat Rev Neurosci* **23**, 744–766 (2022).

44. Amaral, D. G. Emerging principles of intrinsic hippocampal organization. *Curr Opin Neurobiol* **3**, 225–229 (1993).
45. Couey, J. J. *et al.* Recurrent inhibitory circuitry as a mechanism for grid formation. *Nat Neurosci* **16**, 318–324 (2013).
46. Miller, E. K., Erickson, C. A. & Desimone, R. Neural mechanisms of visual working memory in prefrontal cortex of the macaque. *J Neurosci* **16**, 5154–5167 (1996).
47. Noorman, M., Hulse, B. K., Jayaraman, V., Romani, S. & Hermundstad, A. M. Maintaining and updating accurate internal representations of continuous variables with a handful of neurons. *Nat Neurosci* **27**, 2207–2217 (2024).
48. Jochems, A. & Yoshida, M. A robust in vivo-like persistent firing supported by a hybrid of intracellular and synaptic mechanisms. *PLoS One* **10**, e0123799 (2015).
49. Gothard, K. M., Skaggs, W. E., Moore, K. M. & McNaughton, B. L. Binding of hippocampal CA1 neural activity to multiple reference frames in a landmark-based navigation task. *J Neurosci* **16**, 823–835 (1996).
50. Ballinger, E. C., Ananth, M., Talmage, D. A. & Role, L. W. Basal Forebrain Cholinergic Circuits and Signaling in Cognition and Cognitive Decline. *Neuron* **91**, 1199–1218 (2016).
51. Wang, M. *et al.* Neuronal basis of age-related working memory decline. *Nature* **476**, 210–213 (2011).
52. Martin, M. M. & Wallace, D. G. Selective hippocampal cholinergic deafferentation impairs self-movement cue use during a food hoarding task. *Behav Brain Res* **183**, 78–86 (2007).
53. Croxson, P. L., Kyriazis, D. A. & Baxter, M. G. Cholinergic modulation of a specific memory function of prefrontal cortex. *Nat Neurosci* **14**, 1510–1512 (2011).
54. Puram, S. V. *et al.* A TRPC5-regulated calcium signaling pathway controls dendrite patterning in the mammalian brain. *Genes Dev* **25**, 2659–2673 (2011).
55. Kadir, S. N., Goodman, D. F. M. & Harris, K. D. High-dimensional cluster analysis with the masked EM algorithm. *Neural Comput* **26**, 2379–2394 (2014).
56. Hattori, S., Chen, L., Weiss, C. & Disterhoft, J. F. Robust hippocampal responsivity during retrieval of consolidated associative memory. *Hippocampus* **25**, 655–669 (2015).
57. Skaggs, W., McNaughton, B. & Gothard, K. An Information-Theoretic Approach to Deciphering the Hippocampal Code. in *Advances in Neural Information Processing Systems* (eds. Hanson, S., Cowan, J. & Giles, C.) vol. 5 (Morgan-Kaufmann, 1992).
58. Guardamagna, M., Stella, F. & Battaglia, F. P. Heterogeneity of network and coding states in mouse CA1 place cells. *Cell Rep* **42**, 112022 (2023).
59. McHugh, T. J., Blum, K. I., Tsien, J. Z., Tonegawa, S. & Wilson, M. A. Impaired Hippocampal Representation of Space in CA1-Specific NMDAR1 Knockout Mice. *Cell* **87**, 1339–1349 (1996).

506 # Tables

507

508 **Table 1. Comparisons of passive membrane properties**

	RMP (mV)	Resistance (MOhm)	Adaptation Index	Intrinsic Excitability (Hz)			
				50 pA	100 pA	150 pA	200 pA
Non-injected	-64.19 ± 0.18	163.31 ± 4.82	0.43 ± 0.02	5.09 ± 0.48	20.45 ± 0.69	29.55 ± 0.71	39 ± 0.54
Scrambled	-64.20 ± 0.21	180.66 ± 2.72	0.53 ± 0.02	2.5 ± 0.35	13.71 ± 0.56	25.21 ± 0.64	33.21 ± 0.82
TRPC4 KD	-63.79 ± 0.25	173.85 ± 2.62	0.67 ± 0.03	7.86 ± 0.49	*22.71 ± 0.59	30.5 ± 0.70	36.57 ± 0.65

509

510 RMP: resting membrane potential, Resistance: input resistance, Adaptation index: firing rate adaptation

511 index.

512

513

514 # Methods

515 **Animals**

516 Twelve-week-old C57BL6/J male mice were obtained from a local animal facility. The mice were
517 group-housed until the time of surgery and individually housed thereafter to avoid injury to sutures
518 and/or implants. A 12-h light/dark cycle was used, and the mice underwent experiments during the light
519 cycle. Mice housing room conditions were maintained at 21–24°C and 40–50% humidity. All
520 experimental procedures were performed in accordance with animal research permission (TVA)
521 obtained from the animal committee of Sachsen-Anhalt (Landesverwaltungsamt Referat
522 Verbraucherschutz, Veterinärangelegenheiten, Az. 42502-2-1388 DZNE, 203.m-42502-2-1665
523 DZNE).

524

525 **TRPC4 channel knockdown**

526 We developed a TRPC4 shRNA-expressing virus (TRPC4_AAV_U6_shRNA2_GFP) to knock down
527 TRPC4 channels and a scramble virus (AAV_U6_scramble_GFP) for the control experiments. Oligos
528 for TRPC4 were designed based on Puram and colleagues[54] and were ordered from Sigma-Aldrich. The
529 following oligonucleotides were used to clone siRNA against mTRPC4 into AAV_U6_GFP:

530 mTRPC4_siRNA2: siRNA_TRPC4_Mouse/Human_2: Sense and antisense

531 5'- GATCC GGTCAGACTTGAACAGGCAA TTCAAGAGA

532 TTGCCTGTTCAAGTCTGACC TTTTTTG – 3'

533 3'- G CCAGTCTGAACTTGTCCGTT AAGTTCTCT AAC-GGACAAGTTCAGACTGG

534 AAAAAACTTAA-5'

535 Adeno-associated virus (AAV2) and U6 were used as the vectors and promoters, respectively. After
536 purification, the titers were checked by qPCR (using TaqMan probes) and different dilutions. The titer
537 for TRPC4_AAV_U6_shRNA2_GFP was $4.03*10^{12}$ and for AAV_U6_scramble_GFP was $3.56*10^{12}$.
538 Finally, primary hippocampal cell cultures were infected with either no virus, scrambled virus, or
539 TRPC4 KD virus, and a significant reduction in TRPC4 mRNA expression by the TRPC4 KD virus

540 was confirmed by RT-qPCR (Fig. 1A).

541

542 **Surgery**

543 C57BL/6JCrl male mice were weighed and anesthetized using a ketamine and xylazine cocktail
544 (ketamine 20 mg/mL + xylazine 2.5 mg/mL, 0.1 mL/20 g). The head was fixed in the stereotactic device
545 approximately 10 min after anesthetic injection. Head hair was completely removed, and the head was
546 scrubbed using betadine (povidone-iodine) and ethanol 70%. A small incision was made using a scalpel,
547 and the tissues were gently retracted. The skull position was checked horizontally. The Bregma point
548 was used as reference, and the injection sites were marked according to coordinates from Paxinos atlas
549 (AP: -2.1, ML±1.7, DV: 1.1 and AP: -2.7, ML±2.5, DV: 1.5). The marked points were drilled with a
550 0.7 mm drill tip. TRPC4_AAV_U6_shRNA2_GFP or AAV_U6_scramble_GFP viral particles were
551 injected using a Hamilton neuro syringe (1701, 33 g needle) and stereotaxic syringe pump (CHEMYX,
552 NANOJET) to control injection speed (100 nL/min) and volume (1 uL/site). The needle remained at the
553 injection site for 5 min before retraction. Next, the skin was closed using veterinary surgery glue, and
554 carprofen (5 mg/kg) was subcutaneously injected. Metamizole (200 mg/kg) was added to a 100 mL
555 water bottle. The mice were allowed to recover for a few hours in the surgery room and then transferred
556 to the animal room. They were checked daily (for three days) for recovery and pain management.
557 For *in vivo* electrophysiological experiments, a microdrive with eight tetrodes was implanted on the
558 right hemisphere and lateral to the virus injection site (AP: -2.1, ML±1.8, DV: 0.6). Four anchor screws
559 and one ground screw are affixed to the skull. The implant was fixed using acrylic dental cement.

560

561 ***In vitro* neural recordings**

562 The mice were deeply anesthetized with isoflurane, and the brains were quickly extracted after
563 decapitation. Brains were placed in ice-cold cutting solution (110 mM) 110 Choline Cl, 7 mM MgCl2
564 (6H2O), 0.5 CaCl2, 2.5 KCl, 25 glucose, 1.2 NaH2PO4, 25 mM NaHCO3, 3 mM pyruvic acid, 11.5
565 ascorbic acid, and 100 mM D-mannitol). A Leica VT-1000 vibratome was used to obtain 350 μM
566 coronal slices. Brain slices were transferred to a holding chamber containing normal ACSF (nACSF)
567 (126 mM) (126 mM NaCl, 1.2 mM NaH2PO4, 26 mM NaHCO3, 1.5 mM MgCl2, 1.6 mM CaCl2, 3

568 mM KCl, and 10 mM glucose). Slices were submerged for 30 min at 37 °C and then transferred to
569 another holding chamber at room temperature for at least 30 min before recording.
570 Brain slices were transferred to the recording chamber and continuously superfused with
571 nACSF (34.5 ± 1.5°C). The cells were visualized using an upright microscope (Olympus BX51WI)
572 with a 40x water immersion objective and a Thorlabs CS895MU monochrome camera. GFP+ cells were
573 located by exciting GFP with a 470 nm wavelength LED (CoolLED PE 4000) through a filter cube with
574 excitation filter 469 ± 17.5 nm, dichroic 452–490 nm / 505–800 nm, and emission filter 525 ± 19.5 nm.
575 Whole-cell configuration was achieved using 3–5 MΩ patch pipettes filled with intracellular solution
576 (in mM: 120 K-gluconate, 10 HEPES, 0.2 EGTA, 20 KCl, 2 MgCl2, 7 PhCreat di(tris), 4 Na2ATP, and
577 0.3 Tris-GTP (pH adjusted to 7.3 with KOH). For labeling purposes, 0.1% biocytin was added to the
578 intracellular solution. Access resistance was monitored and compensated for several times during
579 recording. The liquid junction potential was not corrected. Electrophysiological signals were amplified
580 using a Multiclamp 700A amplifier and digitized using an Axon Digidata 1550 B. Current clamp
581 recordings were routinely filtered at 10 KHz and sampled at 20 KHz using pClamp 11 software. After
582 recording, the slices were stored at 4°C in a phosphate-buffered saline (PBS) solution with 4%
583 paraformaldehyde (PFA).
584
585 **Behavioral task**
586 The spatial working memory task in the T-maze was started four weeks after virus injection. Before this
587 test, the mice were handled for three days to habituate to the experimenter. Mice were food-deprived at
588 the start of handling to motivate them for the reward, and reward pellets were introduced to them before
589 starting the main experiment. Animal weight was maintained between 85–90% of body weight before
590 food deprivation. Second, habituation to the T-maze (OHARA Ltd., Japan) was performed for three
591 days.
592 Each animal was tested for 10 days, with each day constituting 10 trials (10 sample +10 choice
593 phases). Each trial started with a sample trial (forced trial), in which the T-maze software assigned the
594 left or right door (at the T-junction) to open randomly. First, the start door was opened, and the mouse
595 moved from the start area to the stem, open arm (top of the T-maze), and goal area where it received

596 the reward. Next, the animal returned to the start area using the return arm and waited for 30 s (delay
597 period). After the delay, the choice trial began; this time, both the left and right arms were open, and
598 the mouse chose the arm opposite the sample trial. If the trial was successful, the animal received a
599 pellet at the goal location. After collecting the reward, the animal moved back to the start area, where a
600 new trial began after 45 s (inter-trial interval, ITI). After each experiment, the maze floor was cleaned
601 with 10% ethanol, and the walls were cleaned with water. Behavioral data were analyzed using
602 MATLAB (MathWorks) and SPSS (GEE).
603
604 ***In vivo* neural recordings**
605 Tetrodes were made using 12.5 μm Tungsten wire (California Fine Wire Co.) and grouped in a single
606 bundle with eight tetrodes (32 channels) inside a microdrive (AXONA). The tetrodes were gold-plated
607 using nanoZ (White Matter LLC, USA) in gold solution to reduce the impedance to 150 kΩ.
608 Screening was conducted 7–10 days after surgery and after handling the animals to place the
609 tetrodes in the pyramidal layer of CA1. Screening was performed in an open-field arena (30 × 30 cm,
610 shielded and grounded). The presence of place cells, autocorrelation, firing frequency, and waveform
611 characteristics were the criteria used to identify the pyramidal layer. Once the tetrodes were in a position
612 or very close to CA1, the behavioral experiment in the T-maze began.
613 Single-unit activity and local field potentials (LFP) were recorded using an in vivo
614 electrophysiology setup (Axona Ltd.). The data were recorded in the raw mode at a sampling rate of 48
615 kHz. To obtain single-unit spike data, raw data were referenced and band-passed (400–8000 Hz) using
616 custom scripts written in MATLAB (MathWorks), and spikes were detected using TINT (Axona Ltd.).
617 The detected spikes were clustered using KlustaKwik[55] for automatic clustering, and manual curation
618 of the clusters was performed using the Klusters software (Lynn Hazan). LFP data with a 4800 Hz
619 sampling rate were created using TINT (Axona Ltd.). The position of the mouse was tracked at 50 Hz
620 using a video camera that recorded the position of a light-emitting diode attached to the mouse head.
621
622 **Histology**

623 Mice were anesthetized with a ketamine and xylazine cocktail and transcardially perfused with cold
624 PBS (4°C, 15 mL) and then cold paraformaldehyde 4% (PFA, PH~7.4, 50 mL). Brains were removed
625 and post-fixed in PFA 4% at 4°C for 24 h. After applying the cryoprotective protocol (one day in sucrose
626 10%, three days in sucrose 30%), samples were embedded in cubic molds filled with Optimal Cutting
627 Temperature compound (O.C.T.) and then snap frozen. Next, the samples were transferred to the -80°C
628 freezer for storage. The fixed samples were sectioned using a cryostat. The slices were then covered
629 and mounted using a mounting medium. Images were obtained with a confocal microscope (Zeiss,
630 AxioImager M2) and fluorescence microscope (Keyence, BZ-X710) using 2.5x, 5x, and 40x objectives
631 to control for virus expression and tetrode traces (Supplementary Fig. 1).
632
633 ***In vitro* data analysis**
634 The resting membrane potential was measured by averaging the membrane potential for 1 min after seal
635 opening without current injection. Input resistance was calculated using Ohm's law, measuring the
636 voltage deflection in response to a negative current pulse of -50 pA at -65 mV. Intrinsic excitability was
637 evaluated by counting the number of action potentials during the positive step-wise current injections
638 (1 s), from -300 to 300 pA in 50 pA jumps (IV protocol). The adaptation index was calculated by
639 dividing the instantaneous frequency of the last pair of action potentials by the instantaneous frequency
640 of the second pair of action potentials in the first sweep, with at least 10 action potentials in the IV
641 protocol. *In vitro* persistent firing was induced by a 2 s 100 pA current injection at a voltage level of 5–
642 3 mV below the action potential threshold. The strength of persistent firing was evaluated by calculating
643 the average firing frequency and depolarization in the first 10 s post-stimulus. The cells were classified
644 as having long (> 30 s), short (< 30 s), or no persistent firing, based on the duration of persistent firing
645 observed (measured from the offset of the stimulus).
646
647 ***In vivo* data analysis**
648 The data were analyzed using custom-written MATLAB scripts and the CMBHome toolbox developed
649 at the Center for Memory and Brain, Boston University.
650

651 *Temporal binning and Z-score firing rate*

652 The time-binned firing rate of each cell was prepared using a 0.5 s bin and smoothed with a 2.5 s
653 Gaussian window to analyze *in vivo* persistent firing. The Z-scored firing rate was calculated from the
654 time-binned firing rate data using the following equation:

655 $$Z = (f - mean(F))/std(F),$$

656 where *f* and F are the binned firing rates from the period of interest and baseline period, respectively.

657

658 *Cell type classification based on activity change*

659 Neurons were classified into activated (Act), suppressed (Sup), and non-modulated (NM) cells,
660 according to the delay period activity[56] (Fig. 2E). The binned firing rate at baseline (15–5 s before the
661 delay) was compared to the activity during the delay (0–25 s) using the Wilcoxon rank-sum test (WRS).
662 Cells were considered to be modulated if the test result was significant ($p < 0.01$). The z-value obtained
663 during the test (WRS z-value) was used to classify the modulated cells into the Act (WRS z-value >
664 2.58) and Sup (WRS z-value < -2.58) groups. The remaining cells were classified as NM. The WRS z-
665 values were used to plot a histogram, as shown in Fig. 2E.

666

667 *Temporal field*

668 The peak z-scored firing rate during the delay period was determined to define the temporal field for
669 each cell. The temporal field duration was defined as the time when the z-scored firing rate was
670 continuously above 10% of the peak value (Fig. 2I). In Fig. 3, the temporal field duration is defined in
671 the same way, using the raw firing rate instead of the z-scored firing rate.

672

673 *SVM analysis*

674 A population vector was built for each trial of each session using neuronal activity during the delay
675 period (0–25 s) or from the goal area (0–10 s). Single-unit spike activity was temporarily binned (0.5 s
676 bin) for left vs. right and ITI vs. delay comparisons. A temporal bin size of 0.02 s was used for the left
677 vs. right goal comparison with a 5 s sliding window (Fig. 6F and G). Each trial was then labeled

678 according to the type of test: ITI vs. delay or left vs. right (retrospective or prospective). Only sessions
679 with at least 15 units were included in the analysis.

680 Binary SVM comparisons were performed for each session with the fitcsvm function
681 (MATLAB) using a linear kernel and two-fold cross-validation of the input data to evaluate model
682 performance. The model was run 30 times, and the obtained balanced accuracies were averaged. To
683 evaluate the significance of the prediction, the class labels were scrambled, and the SVM model was
684 run for the non-scrambled data a minimum of 30 times (sessions where label permutation did not
685 generate at least 30 different combinations were not included in the analysis). Moreover, a random
686 accuracy distribution was built and then used to determine the z-scored balance accuracy. Sessions with
687 z-score > 1.96 were considered to have above-chance accuracy.

688

689 *Spatial information and place cells*

690 Spatial information (SI) is defined as the extent to which the firing of a cell can be used to predict the
691 position of the animal. The SI was calculated using the formula of Skaggs et al. (1992)[57]:

692 $$SI = \int_{\infty} \lambda(x) log_2 \frac{\lambda(x)}{\lambda} p(x) dx,$$

693 where SI is the information rate in bits/s, x is the spatial location of the animal, λ(x) is the mean
694 frequency at location x, p(x) is the probability of finding the animal at a given location in the maze, and
695 λ is the overall firing rate of the cell.

696 Spatially modulated cells were selected by building a randomized distribution of spatial
697 information values obtained by circularly shifting the spike timing and position vectors for at least 20 s
698 100 times. Cells with spatial information above the top 95% of the random distribution were considered
699 spatially modulated cells (place cells).

700 The spatial rate maps represent the average firing rate of a cell at a given location, and were
701 obtained by dividing the number of spikes at a location by the total time that the animal spent at that
702 location (occupancy). Rate maps were calculated using 1x1 cm bins, and the data were smoothed using
703 a two-dimensional convolution with a Gaussian kernel with a 2.5 cm standard deviation. Only bins with
704 speed greater than 2.5 cm/s were considered in the calculation.

705 Place field centers were detected as follows. First, pixels of a rate map with a high firing rate
706 (> 4 SD) were extracted. Extracted rate map was processed with the regionprops function (MATLAB)
707 to detect and characterize the individual fields and the area and centroid parameters were obtained. To
708 avoid detecting noise, fields smaller than 12 or larger than 650 cm^2 were discarded, and firing field with
709 the highest coefficient of variation was considered the main firing field of a given neuron. The
710 coefficient of variation was calculated as follows:
711

712 $$CV = \frac{Mean\ field\ firing\ rate}{SD\ field\ firing\ rate}$$

713

714 *Theta amplitudes*

715 Theta components were extracted by bandpass filtering of the LFP data (6-10 Hz). The theta amplitude
716 was calculated using the absolute value of the Hilbert transform of the filtered signal.
717

718 *Putative cell type classification*

719 Putative pyramidal neurons and interneurons were identified based on the average firing rate and spike
720 duration. Cells with an average firing rate < 8 Hz and a peak-to-peak spike duration > 0.255 ms were
721 classified as putative pyramidal cells, whereas those with an average firing rate > 8 Hz and a peak-to-
722 peak spike duration < 0.255 ms were classified as putative interneurons[58,59].
723

724 *Trial selection for goal analysis*

725 The duration of time animals stayed at the goal areas varied greatly from trial to trial, ranging from 1.6
726 to 410.0 s (median duration: 47.74 and 47.73 s for control and TRPC4 KD groups, respectively; WRS
727 test, p = 0.99), because the task did not restrict the time animals spend at the goal areas. In addition, the
728 animals returned to the top arm (top of T) in some trials. Therefore, we limited our goal analysis to trials
729 in which the animals continuously spent at least 10 s within the goal area during the sample phase.
730 When multiple such periods were found in a trial, we analyzed the first incident. The baseline period to
731 build the z-scored firing rate was the last 20 s of the ITI period before goal entry. This ensured that goal

activity was not included in the baseline period. In Fig. 6A, H, and K, the black vertical gap separates the first 10 s, which is referenced to the end of the ITI period, from the rest, which is referenced to the start of goal entry. The trials in each recording session were first divided into left and right sample goal trials to compare correct and incorrect trial activities. Subsequently, we checked whether at least one correct or incorrect trial was present for each goal location. Sessions that did not meet these criteria were excluded from the analysis.

Statistical analysis

The data were checked for distribution and homogeneity before statistical analysis. Comparisons between groups were performed using the Wilcoxon rank-sum and Kruskal–Wallis tests. A t-test or analysis of variance (ANOVA) followed by Tukey's post-hoc test was used for normally distributed data. Multiple-comparison corrections were used where relevant. Categorical variables (group ratios) were compared using the chi-squared test or Fisher's exact test if any group had fewer than five items. Boxplots represent the median and upper and lower quartiles. Significance was expressed as follows: * $p < 0.05$, ** $p < 0.01$, and *** $p < 0.001$.

Data availability

Data used in the current study will be available on request to the corresponding authors.

Code availability

All source codes used in the current study will be available on request to the corresponding authors.

Acknowledgments

We would like to thank K. Jeffery, S. Leutgeb, J. Leutgeb, M. Brandon, and K. Allen for their help in establishing the in vivo electrophysiological recordings. We thank L. Leichert and O. Stork for their assistance and technical support, and M. Freichel for sharing the TRPC KO mice with us. We thank M. Hasselmo, B. McNaughton, and T. McHugh for their valuable comments on this manuscript. This work

was supported by the Federal State of Saxony-Anhalt and the European Structural and Investment Funds (ESF, 2014–2020, project number ZS/2016/08/80645), the Deutsche Forschungsgemeinschaft projects YO177/4-1, YO177/4-3, and YO177/7-1 (to M.Y.), and the German Center for Neurodegenerative Diseases (to A.D.).

Author Contributions

Conceptualization and experimental design, M.Y. and M.S.; analysis, A.R., M.Y., and B.S.M.; investigation, B.S.M.; writing, M.Y. and A. R.; methodology, A.D. and R.K.; software, M.Y. and F.T.; funding acquisition, M.Y.; supervision, M.Y. and M.S.

Competing interests

The authors declare no competing interests.

Corresponding author

Correspondence and requests for materials should be addressed to motoharu.yoshida@lin-magdeburg.de.

Extended data Figures

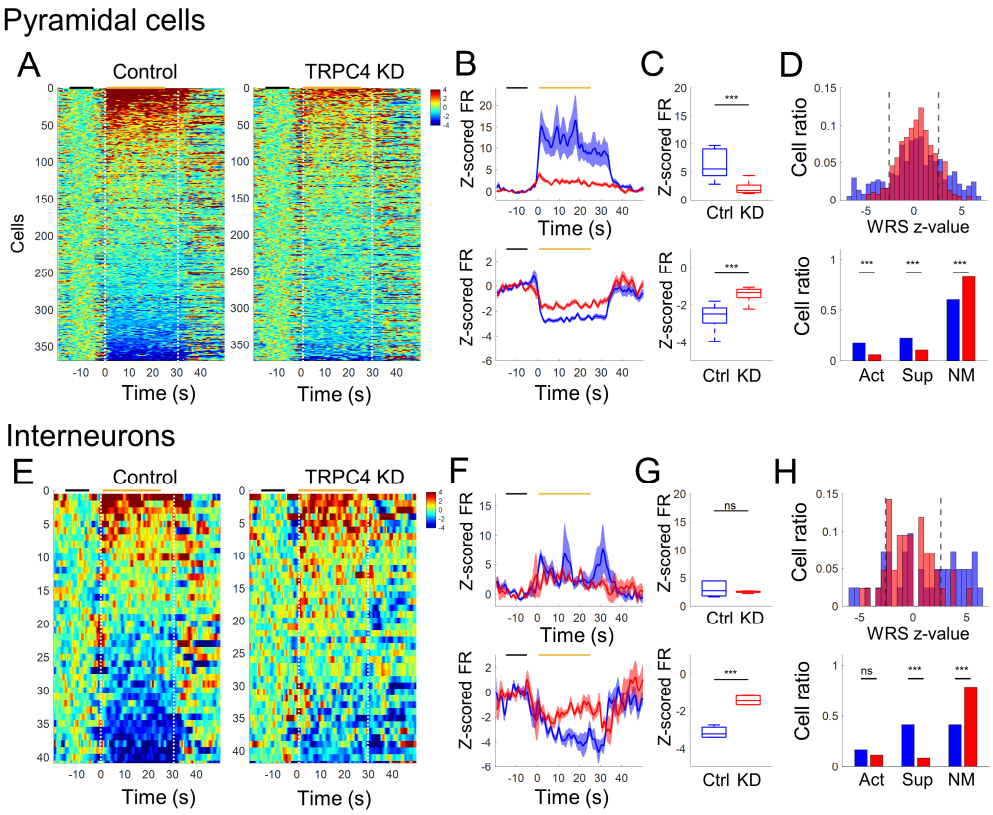

Extended Data Fig. 1 Activity of pseudo pyramidal and interneurons (A) Z-scored firing rate of pseudo-pyramidal cells sorted by the delay period activity. Black and orange horizontal lines at the top of each panel indicate baseline period and period for cell sorting, respectively. (B) Averaged z-scored firing rate (FR) of top (upper panel) and bottom (lower panel) 10% cells in A. (C) Comparison of z-scored firing rate of the top (upper panel; Wilcoxon rank sum Test, $p < 0.001$) and bottom (lower panel; Wilcoxon rank sum test, $p < 0.001$) 10 % cells in A during the delay period (0-25 s). (D) Classification of activated (Act), suppressed (Sup) and non-modulated (NM) cells using Mann–Whitney U (MWU) test. The upper panel shows the distribution of Wilcoxon rank-sum z-values and the lower panel shows the ratio of cells in each category (WRS test, $p < 0.001$ for all groups). (E to H) Same as A to D but for pseudo-interneurons. Statistical tests in G: WRS test, $p = 0.6905$ in the upper panel, and $p < 0.001$ in the lower panel.

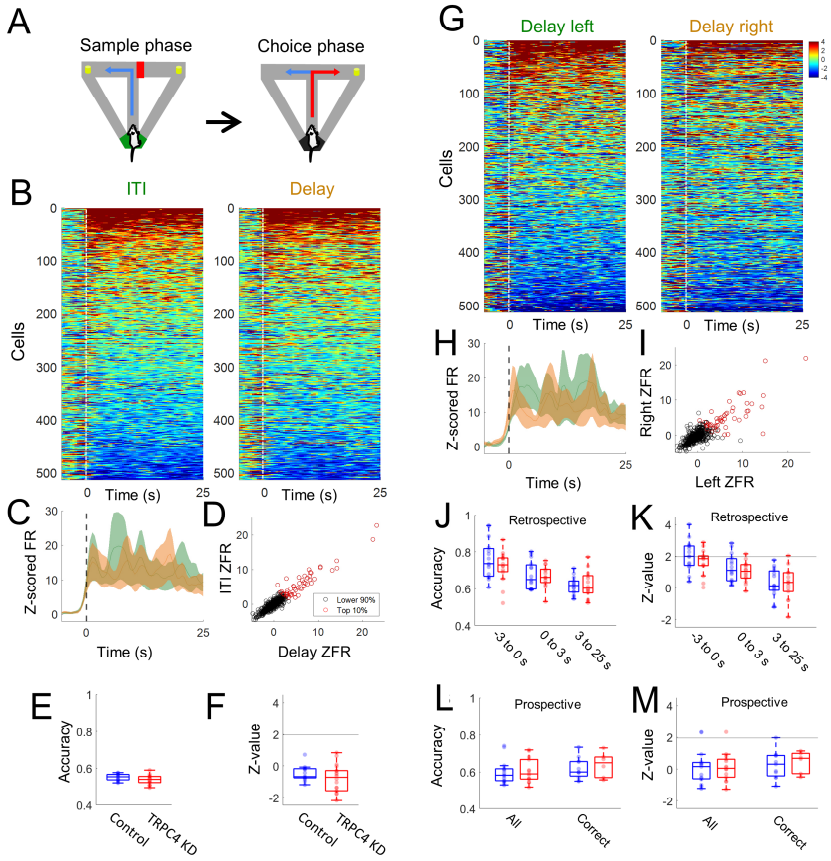

Extended Data Fig. 2. Persistently firing cells do not strongly code task phases and direction of turn (A) Inter-trial-interval (ITI, green) in the sample phase and delay period (orange) in the choice phase. Animals were in the same start box in the ITI and delay period. (B) Z-scored firing rate of all cells sorted by the averaged activity during the ITI (0–25 s) in both ITI and delay. Vertical dashed lines indicate the onset of ITI or the delay period. Baseline and sorting period were the same as in Fig. 2B. (C) Averaged activity of the top 10% cells in B from ITI (green) and delay period (orange; WRS test, p = 0.40). (D) Comparison of activity during ITI and the delay period from all cells. Each circle corresponds to a cell. The top 10% cells (based on common sorting) are indicated by red circles. (E-F) Accuracy (E) and z-value (F) from the SVM prediction of ITI vs delay phase based on the activity of all cells (WRS test, p = 0.61 and p = 0.59 for E and F, respectively). The horizontal line in F indicates a 5% significance level. (G) Z-scored firing rate of all cells near the delay period, sorted by the average activity of the left trials. Here, the left and right trials are defined by the direction of the turn at the sample phase (retrospective coding). (H) Averaged activity of the top 10 % cells in G from the left (green) and right (orange) trials. (WRS test, p = 0.0058). (I) Comparison of activity from left and right trials for all cells. Each circle corresponds to a cell. The top 10% cells (based on common sorting) are indicated by the red circles. (J-K) Accuracy (J) and z-value (K) from the SVM prediction of left vs right trials based on the activity of all cells at different segments before (-3 to 0) and during (0 to 3s, 3 to 25 s) the delay period (WRS test, p = 0.49, 0.91 and 1 in J; p = 0.20, 0.28 and 0.98 in K). (L-M) Accuracy (L) and z-value (M) from the SVM prediction of future left vs right trials based on the activity of all cells during (3 to 25 s) the delay period (prospective coding). This analysis was done using all (correct and wrong) and only correct trials (WRS test, p = 0.98 and p = 0.59, respectively, in L; WRS test, p = 0.78 and p = 0.52, respectively, in M). SVM, support vector machine

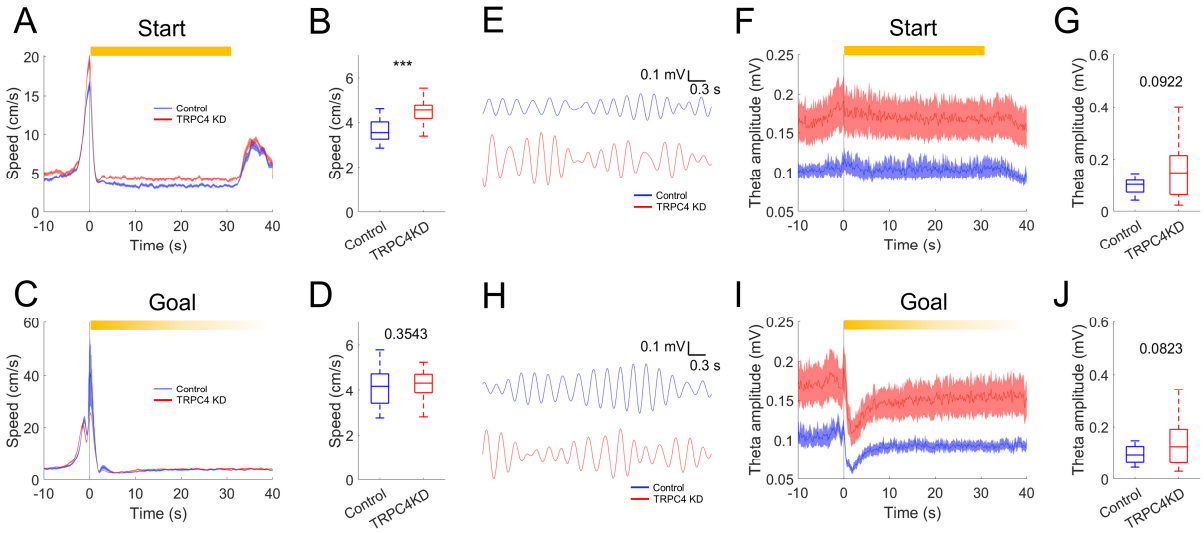

Extended Data Fig. 3 Running speed and theta amplitude at the start and goal areas (A) Average running speed of control and TRPC4 KD animals at the start area. Time is relative to the entry to the start area. This figure includes both the sample (ITI) and choice (delay) phases. (B) Comparison of the speed in the start area (Wilcoxon rank sum test, $p < 0.001$). (C) Same as A but for the goal area. Note that there was no set duration during which animals stayed at the goal area. While we show 40 s of goal speed data, animals were already out of the goal areas in some trials. (D) Comparison of the speed in the goal area (Wilcoxon rank sum test, $p = 0.35$). For this comparison, the speed of each session was calculated using only the time the animal stayed in the goal area. (E) Examples of filtered theta oscillation at the start area. (F) Theta amplitudes of control and TRPC4 KD animals at the start area. (G) Comparison of the averaged theta amplitudes in the start area (Wilcoxon rank sum test, $p = 0.092$). (H) Examples of filtered theta oscillation at the goal area. (I) Theta amplitudes of control and TRPC4 KD animals at the goal area. As in C, animals were out of the goal areas in some trials before the end of the trace. (J) Comparison of the theta amplitudes in the goal area (Wilcoxon rank sum test $p = 0.082$). As in D, the theta amplitude of each session was calculated using only the time the animal stayed in the goal area.

780

781 **Supplementary Information**

782

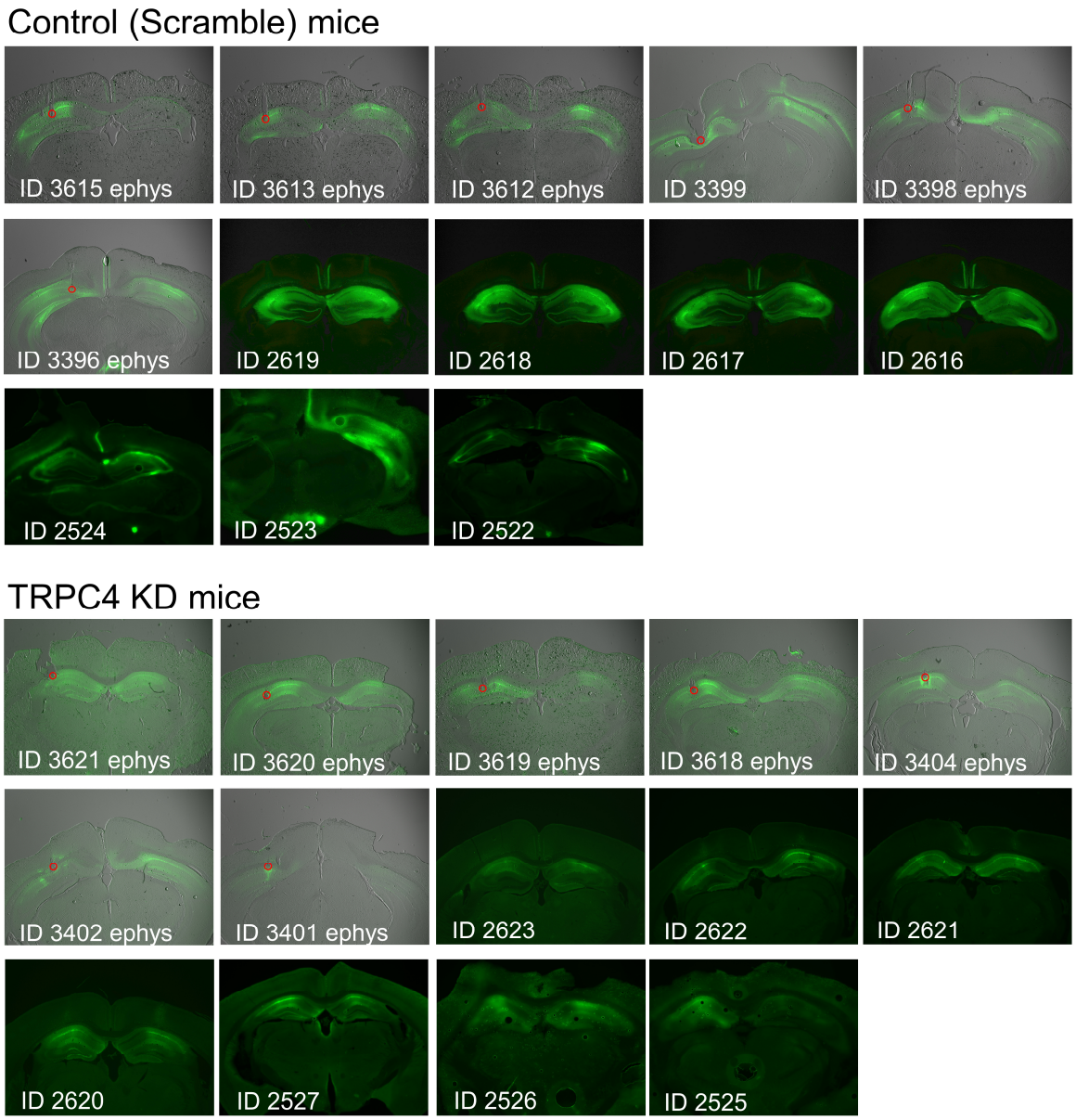

Supplementary Figure 1. Virus expression and tetrode track. GFP expression and track locations of each animal for both the control and TRPC4 KD groups. Animal IDs followed by "ephys" indicate that those mice were used for electrophysiological recording. The tips of tracks are highlighted with a red circle. Other animals were only used for the behavioral test.